Crack Growth Monitoring at CFRP Adhesive Bondings

Wolfgang ADEBAHR [1], Markus RAHAMMER[1], Ronny SACHSE [2],
Peter MIDDENDORF [2] and Marc KREUTZBRUCK [1]
[1] University of Stuttgart, Institut für Kunststofftechnik, Stuttgart, Germany
[2] University of Stuttgart, Institute of Aircraft Design, Stuttgart, Germany

Contact e-mail: wolfgang.adebahr@ikt.uni-stuttgart.de

Abstract. Within the continuous lightweight trend fiber-reinforced plastics, especially carbon-fiber (CFRP), are increasingly used in aerospace and automotive industries. The advantage of such materials compared to metals is extremely high specific stiffness with simultaneous low density. Among the many joining techniques adhesive bonding is the most common and practical one when dealing with composite materials. However, due to critical crack growing in adhesive bonds, joining by riveting is still standard. In this study the crack growth in adhesive bonded CFRP specimens under dynamic tensile stress is monitored by two non-contact NDT techniques: Air-coupled ultrasound in transmission mode and active lockin-thermography evaluated at load frequencies. In case of air-coupled ultrasonic testing, guided waves are generated by slanted transducer-receiver-setup to detect crack propagation. The thermoelastic effect (SPATE) and the mechanical hysteresis is used to generate the temperature difference in the crack-tip for thermography measurements. Both methods give promising results for detecting the current crack front location and the crack growth velocity. While the ultrasonic technique provides a slightly higher accuracy, thermography has the advantage of true online monitoring, because the measurements are made while the cyclic load is being applied. The NDT methods are compared with a visual crack front inspection at the specimen flanks. The results of both approaches show good agreement. As a further important task we investigate the effect of a crack stopper within the specimen on the crack growth. The results show, that regardless of a non-horizontal alignment of the crack fronts, the crack propagation is dramatically reduced near the crack stopper. Additionally, it is shown that clamping is the main effect of the used crack stopper. The results are helpful for further numerical modelling of adhesive bonds and the corresponding predictability of life time and damage tolerance.

Excerpt from ISBN 978-3-00-053387-7

Introduction

Nondestructive testing of carbon fiber reinforced plastics (CFRP) is an integral part in modern aerospace industry. Additionally, the use of CFRP in automobile industry increases significantly. Although adhesive bonding is much better for aerodynamics and load transmission over large areas, so far assembly of two or more different CFRP parts is done by screwing or riveting. Unfortunately, bonded joints make it difficult to stop a crack under continuous strain. Thus, so called crack stoppers are applied.

This paper discusses the analysis of a crack front during cyclic loading in a dynamic test rig. Thereby, the crack front on the outer faces of the specimens is analyzed by optical microscopes, whilst the crack propagation is inspected by thermography and air-coupled ultrasound on the inside.

Theoretical Basics

1.1 Thermography

The generation of thermal waves can be realized by different heating mechanisms. In this paper, both, thermoelastic and hysteresis effect will be discussed.

Whilst loading an object, the thermoelastic effect produces a change in temperature, which is proportional to the applied stress. The relation between change in temperature ΔT, density δ and heat capacity c_p can be found in [2] and [3]. During cyclic loading, the stress-strain-distribution carries out a hysteresis curve where the enclosed area correlates to the lost energy. In this case the change of temperature ΔT_H is related to the stress in a quadratic dependency, assuming the relation between strain ϵ_r and stress σ is linear [4]. During cyclic loading, a thermal wave is generated which can be visualized and recorded on the specimen-surface by a thermography camera. The result is a video sequence onto which a discrete Fourier transformation at a reference frequency is applied pixel by pixel. The outcome is a phase and an amplitude value for every pixel, which can be combined to a phase and an amplitude image showing information in relation to the reference frequency, typically the loading frequency.

1.2 Air-coupled Ultrasound

Coupling an ultrasonic wave into a specimen using air as coupling medium is difficult to achieve due to strong differences in impedance [5]. For transmission, they have to cross several boundary surfaces, i.e. the boundary between transducer and air or the boundary between air and specimen. These boundaries are passed a second time on the way to the receiver. To minimize reflection, ultrasonic transducers for air-coupled ultrasound consist of composite materials [6]. Low density and low speed of sound in the matrix part are leading to a reduction of transducer-impedance. This results in a lower impedance mismatch between transducer and air. To reduce reflection of ultrasound at the interface air/specimen surface, the transducer angle $\theta = 0$ is changed slightly. This slanted transmission mode projects a periodic pressure distribution on the surface of the plate, which leads to a lamb wave. This lamb wave emits air-coupled ultrasound on both sides of the plate in the same angle as the transducer. By x-y-scanning, defects located in the propagation area of the lamb wave can be detected due to influence on the amplitude of the lamb wave, which can be visualized as a C-scan (color-coded amplitude over x-y-coordinates).

Test Procedure

2.1 Preparation of Test Specimen

The “Cracked Lap Shear” (CLS)-specimen consist of a mounting sub plate onto which a second, shorter one, is bonded. Both plates are quasi-isotropic CFRP. A PTFE foil is placed in between the plates, so that initial crack propagation starts at the exact same position for every specimen under load. To inhibit crack propagation, a crack stopper (“Rivetless Nutplate”) is inserted. It consists of bolt, nut and retainer, is placed through the thickness of the specimen and fixed with an adhesive. Two kinds of specimens were made, narrow ones (20 mm width) without and wider ones (40 mm width) with crack stopper.

Excerpt from ISBN 978-3-00-053387-7

2.2 Measuring Methods

The development of the crack length was recorded with two microscope cameras on the right and left side of the specimen. For better detection of the crack front the lateral edges were painted white and a scale was added.

A thermography camera (640 x 512 pixels, NETD <20 mK) was placed on the rear side of the test rig and was focused on the specimen (figure 1). To increase and homogenize the emissivity and to reduce reflections, specimens were painted black for thermography measurements. A video was recorded by the camera during cyclic testing. Afterwards, a discrete Fourier transformation was applied at the loading frequency to get a phase and an amplitude image.

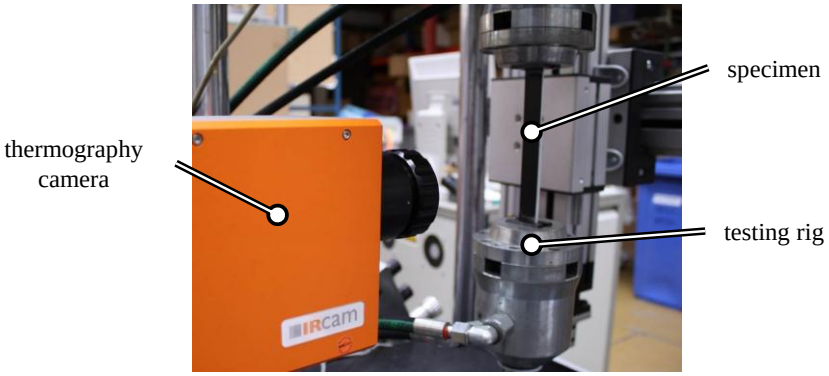

Fig. 1. Thermography measurement set-up.

For measurements with air-coupled ultrasound a test bench with two linear axes was designed. A shield was attached on both sides of the specimen to inhibit ultrasound passing through air directly into the receiver (figure 2). The transducers (Airstar, 200 kHz) can be seen in the figure as well. A C-scan is made by scanning the specimen in two directions and creating a matrix filled with maximum amplitude values true to the x-y-coordinates. Differences in material properties can be revealed in this scan.

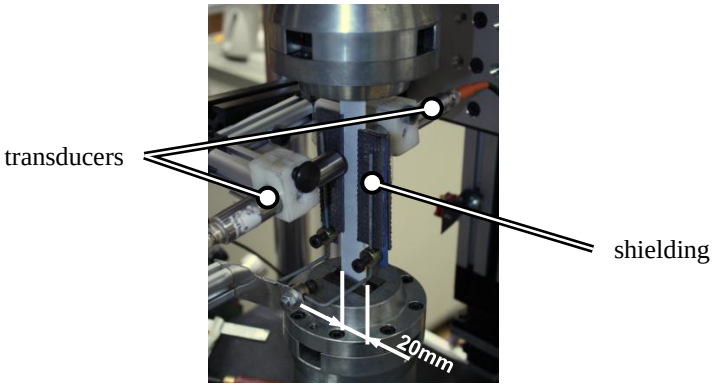

Fig. 2. Test rig and setup with attached shielding.

2.3 Cyclic Loading

The specimens were loaded with a pulsating tensile stress. The maximum load was varied between $F_{max} = 5$ kN and $F_{max} = 20$ kN and the minimum load has been adapted so every measurement was done with a loading ratio of $R = 0.1$ (pulsating tensile stress). The loading frequency was 1 Hz or 5 Hz,, respectively.

Excerpt from ISBN 978-3-00-053387-7

Results

3.1 Thermography Measurements

Thermography measurements had to be done while cyclic loading, since the thermoelastic and the hysteresis effect occur under stress only.

For analysis, phase images are preferred to amplitude images, since phase images show a better signal-noise-ratio. Phase images of specimen CLS-KA-6-2 (without crack stopper) are presented under different loading cycles in figure 3. To define the crack length, the phase image was superimposed every 10^3 loading cycle. In each case the crack length was measured at position $x = 11\ mm$ in the middle of the visible crack front.

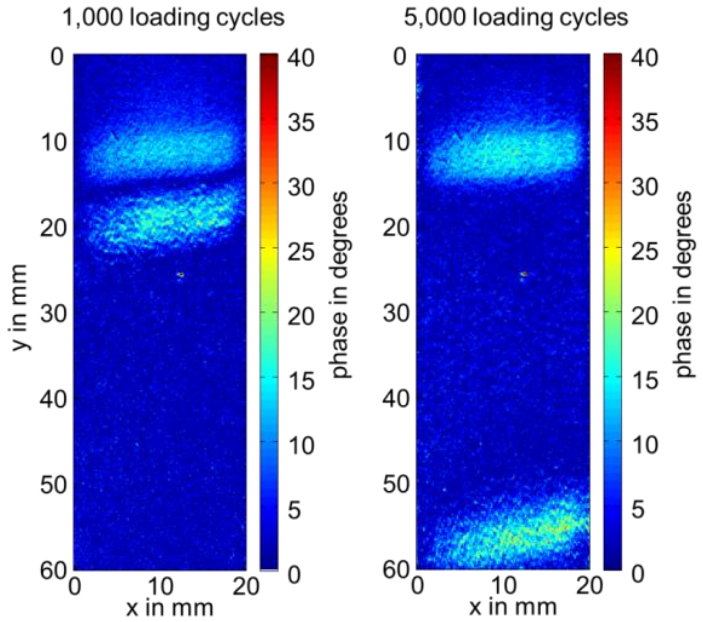

Fig. 3. Specimen CLS-KA-6-2 (without crack stopper), processed phase image at different loading cycles.

The effect of sloped crack fronts with increasing loading cycles is correlated to the results of measurements with the microscope cameras, done in parallel to thermography measurements. In figure 4, right, different crack lengths are shown over loading cycles.

Excerpt from ISBN 978-3-00-053387-7

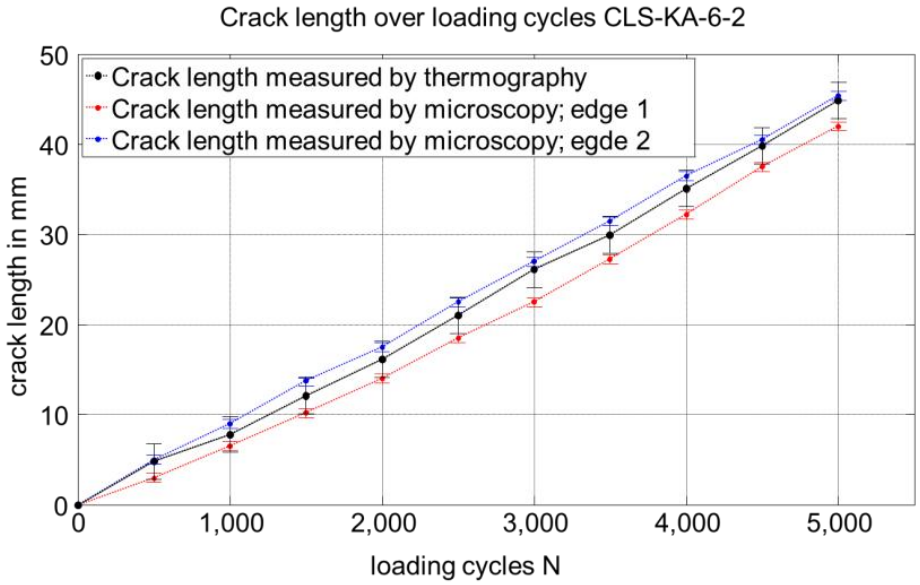

Fig. 4. Specimen CLS-KA-6-2 (without crack stopper), comparison of crack lengths, measured by thermography and microscopy.

Side 1 and 2 refer to the lateral edges of the specimen from where the microscope cameras took their pictures. Crack lengths, measured by thermography are located in between the values measured by the microscope cameras which can be explained by the sloped crack front.

A quantitative analysis of the crack front wasn't feasible for specimens with crack stoppers. This is due to changes in the loading distribution caused by a crack stopper

3.2 Air-coupled Ultrasound Measurements

For ultrasonic testing, the test rig has been stopped temporarily so the measurement could be done without deformation of the specimens. Besides, the shields, which inhibit ultrasound to pass around the specimen, can only be attached while the test rig was standing still.

C-scans of specimen CLS-KA-1-3 (without crack stopper) at different loading cycles are shown in figure 5. The measuring field was adjusted due to the progression of the crack front. Two different areas of varying amplitudes can be distinguished, red for intact areas (bonded CFRP) and blue for delaminated areas. In sound areas, the lamb wave is able to propagate without significant losses. The PTFE foil or an air gap work as a strong barrier, inhibiting signal transmission. To quantify the crack propagation, the middle of the amplitude transition band is used to determine the crack length.

Excerpt from ISBN 978-3-00-053387-7

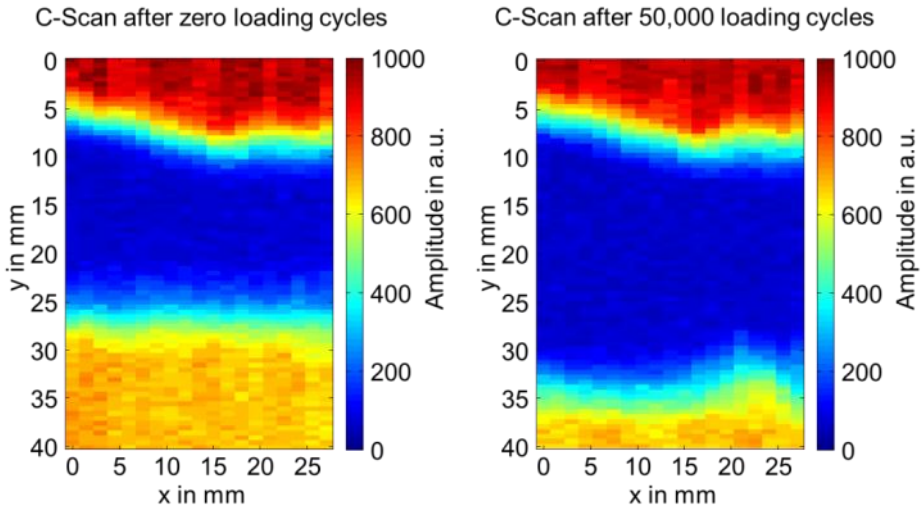

Fig. 5. Specimen CLS-KA-1-3 (without crack stopper), C-scans at 100,000 and 200,000 loading cycles.

Figure 6, shows crack lengths measured by air-coupled ultrasound and microscopy cameras over loading cycles. Crack lengths measured by air-coupled ultrasound are located in between the values measured by microscope cameras. This is due to the fact that the crack front is sloped, thus the crack differs in length at the edges of the specimen. The propagation speed of the crack front is almost constant until it decelerates slightly at 200.000 loading cycles. This is due to the clamping in the test rig. Without clamping, the crack would continue to propagate with constant speed.

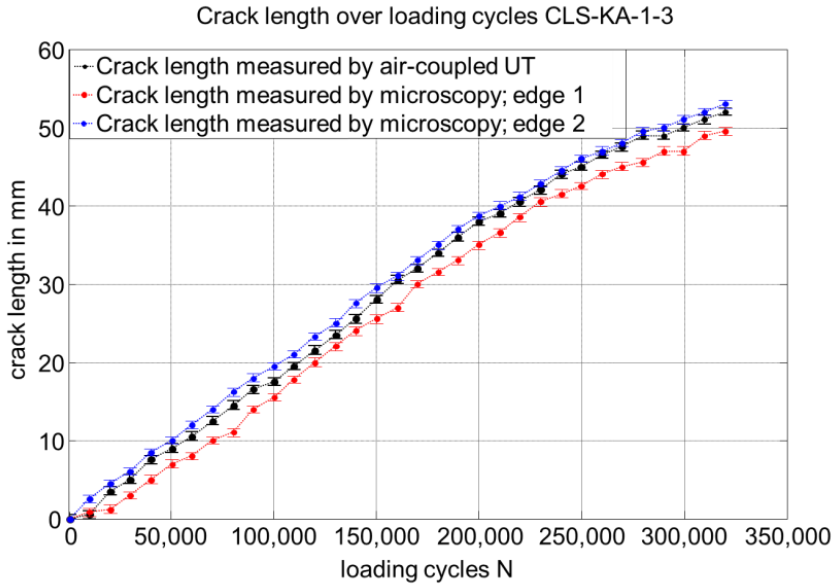

Fig. 6. Specimen CLS-KA-1-3 (without crack stopper), comparison of crack lengths, measured by air-coupled ultrasound and microscopy.

Some specific crack fronts of specimen CLS-KA-4-1 (with crack stopper) are shown at different loading cycles in figure 7. At low loading cycles, the crack front propagates very fast, since the progression is not inhibited. Closer to the crack stopper (52,000 loading cycles) the propagation speed slows down. The results of the microscope cameras confirm, at least at the edges of the specimen, the measurements with air-coupled ultrasound. The shape of the crack front, right and left next to the crack stopper is curved downwards.

Excerpt from ISBN 978-3-00-053387-7

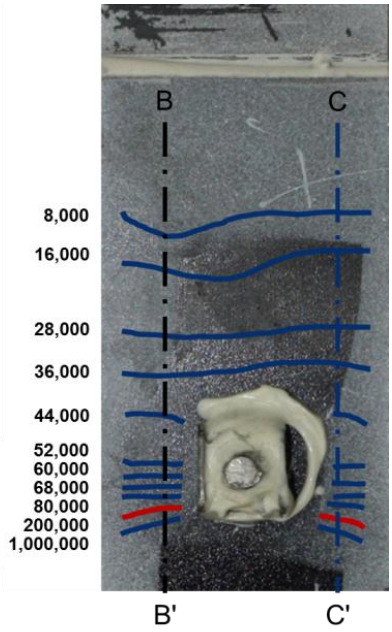

Fig. 6. Specimen CLS-KA-4-1 (with crack stopper) visualized crack lengths at different loading cycles.

The deceleration of the crack propagation is visualized in figure 8. Here the crack length is shown over loading cycles, regarding the segments AA' and BB' from figure 7. Furthermore, the position of the crack stopper is presented as a solid black line. The results of the measurements with ultrasound reveal the efficiency of the crack stopper since it indeed decelerates the crack propagation.

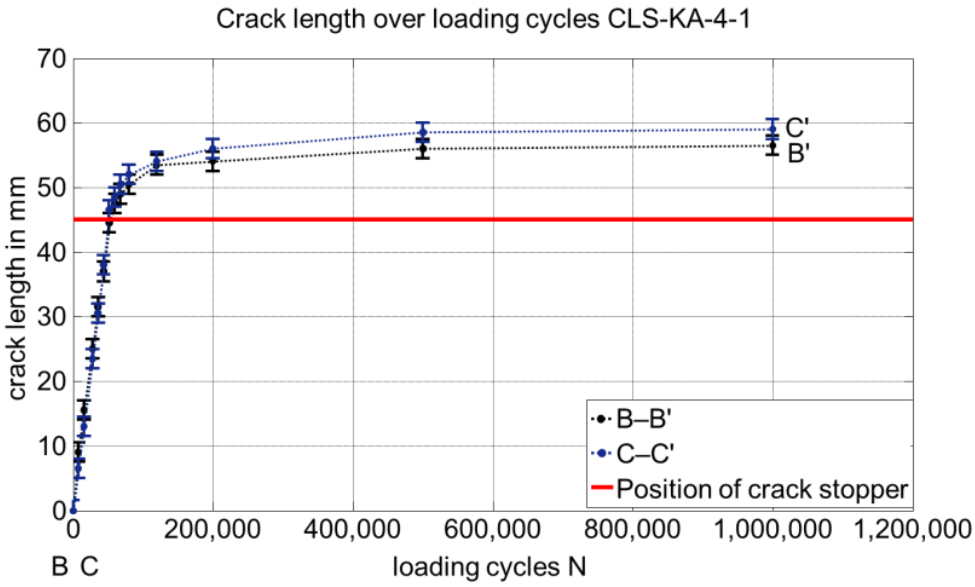

Fig. 7. Specimen CLS-KA-4-1 (with crack stopper), left: visualized crack lengths at different loading cycles, right: crack propagation over loading cycles.

Acknowledgements

The research leading to these results has received funding from the European Community's Seventh Framework Programme (FP7/2007-2013) under grant agreement n° 314180.

Excerpt from ISBN 978-3-00-053387-7

Conclusion and Further Recommendations

Using thermoelastic and hysteresis effect, active thermography allowed the crack front detection of a CLS specimen without crack stopper. Hereby phase images provided a good visualization quality. However the area of the crack front always appears very large so that precise determination of the geometry was not possible. Unfortunately, thermography wasn't feasible for specimens with crack stopper due to changes in the loading distribution caused by the crack stopper.

The crack front and its contour of a specimen without crack stopper could be visualized with air-coupled ultrasound. Assuming the crack front is located in the middle of the amplitude transition band, the determination of the crack length delivered very accurate results. The crack front of a CLS specimen with crack stopper could be visualized via air-coupled ultrasound as well. The efficiency of the crack stopper was proven, since the crack propagation was decelerated after the crack front reaches the crack stopper.

References

[1] M. Käß, "Charakterisierung des Risswachstums und experimentelle Untersuchung eines Riss-Stopper Konzepts für CFK-Klebeverbindungen bei Fatigue-Belastung," Bachelor thesis, University of Stuttgart, 2014.

[2] W. Weber, "Über die spezifische Wärme fester Körper insbesondere der Metall," in *Annalen der Physik und Chemie* (1830), No. 96, pp. 177-213.

[3] D. S. Mountain and J. M. Webber, "Stress Pattern Analysis by Thermal Emission (SPATE)," in: *SPIE* (1978), Nr. 164, pp. 189-196.

[4] I. Solodov, M. Rahammer, D. Derusova, G. Busse, "Highly-efficient and non-contact vibro-thermography via local defect resonance," in Proceedings of the 12th Quantitative Infrared Thermography Conference, Bordeaux, 2014, ID-132.

[5] V. Deutsch, M. Platte and M. Vogt, *Ultraschallprüfung: Grundlagen und industrielle Anwendungen.* (Springer-Verlag, Berlin, 1997).

[6] G. Busse, lecture script "Zerstörungsfreie Werkstoffprüfung", University of Stuttgart, 2011/2012.

[7] D. Döring, "Luftgekoppelter Ultraschall und geführte Wellen für die Anwendung in der Zerstörungsfreien Werkstoffprüfung," Ph.D. thesis, University of Stuttgart, 2011.

[8] S. Gröninger, "Überwachung des Risswachstums in CFK-Klebeverbindungen," bachelor thesis, University of Stuttgart, 2014.

Excerpt from ISBN 978-3-00-053387-7